

Literature Report

Reporter: 许宁
Date: 2021-8-19

Platinum-Triggered Bond-Cleavage of Pentynoyl Amide and *N*-Propargyl Handles for Drug-Activation

Bruno L. Oliveira,^{*,∇} Benjamin J. Stenton,[∇] V. B. Unnikrishnan, Cátia Rebelo de Almeida, João Conde, Magda Negrão, Felipe S. S. Schneider, Carlos Cordeiro, Miguel Godinho Ferreira, Giovanni F. Caramori, Josiel B. Domingos, Rita Fior,^{*} and Gonçalo J. L. Bernardes^{*}



Cite This: *J. Am. Chem. Soc.* 2020, 142, 10869–10880

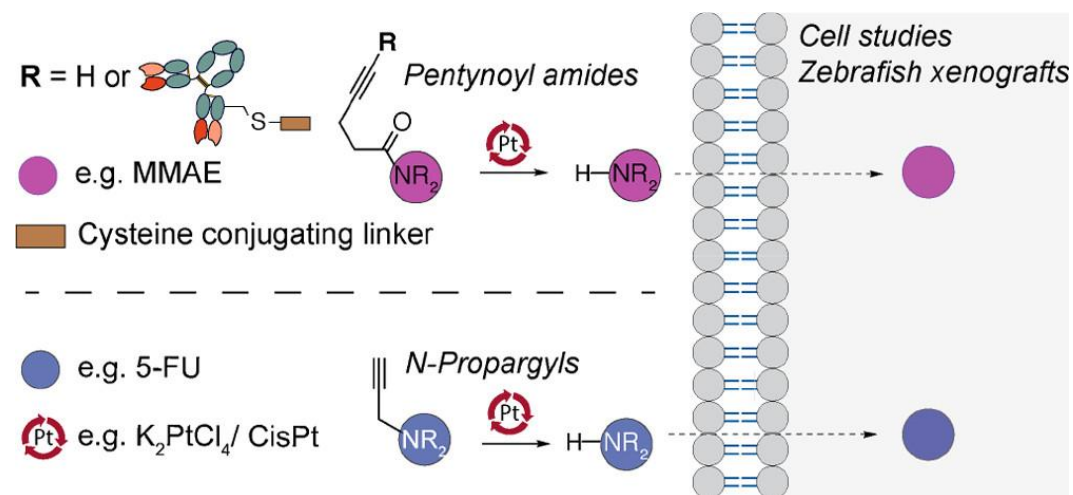


Read Online



Dr Bruno Oliveira
 FCT Stimulus Assistant Researcher

Areas of expertise:
 Protein modification
 chemical-triggered drug activation
 Bioorthogonal chemistry
 bioorganometallic chemistry





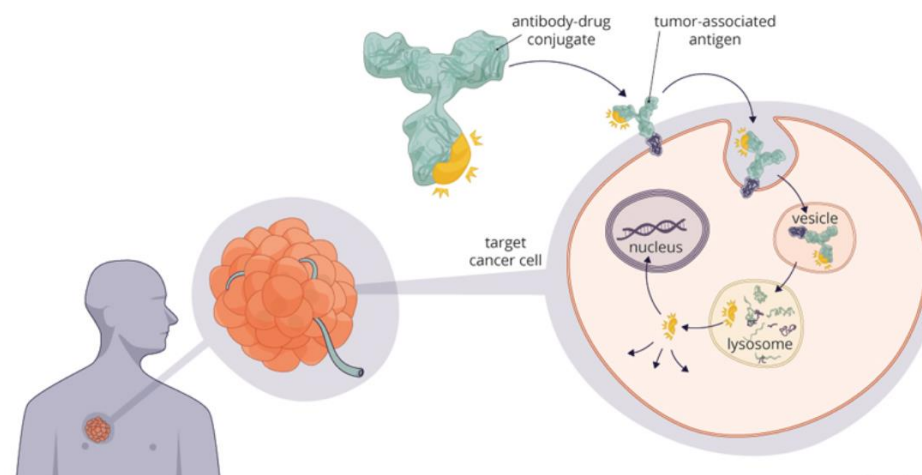
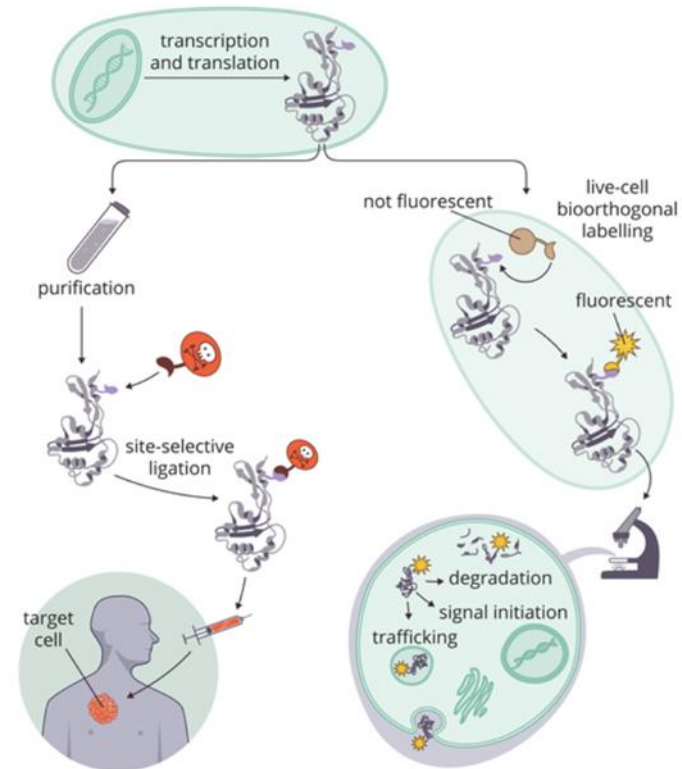
Dr. Gonçalo Bernardes

University of Lisbon, MS, 2004
University of Oxford, Ph D, 2008
ETH, Zürich,
University of Cambridge, 2013
University Lecturer, 2018, 06
Reader, 2019, 06.

GBERNARDESLAB
CHEMISTRY . BIOLOGY . LIFE

Areas of research:

1. Protein conjugation and bioorthogonal labelling
 - 1.1 Site-selective conjugation on purified proteins
 - 1.2 Bioorthogonal labelling of specific proteins in live cells
2. Chemical biology of natural products
3. Delivery gaseotransmitters
4. Synthetic biologics
 - 4.1 Specific delivery of cytotoxics to cancer cells
 - 4.2 Carbohydrate-based Vaccines



Antibody–drug conjugates (ADCs)

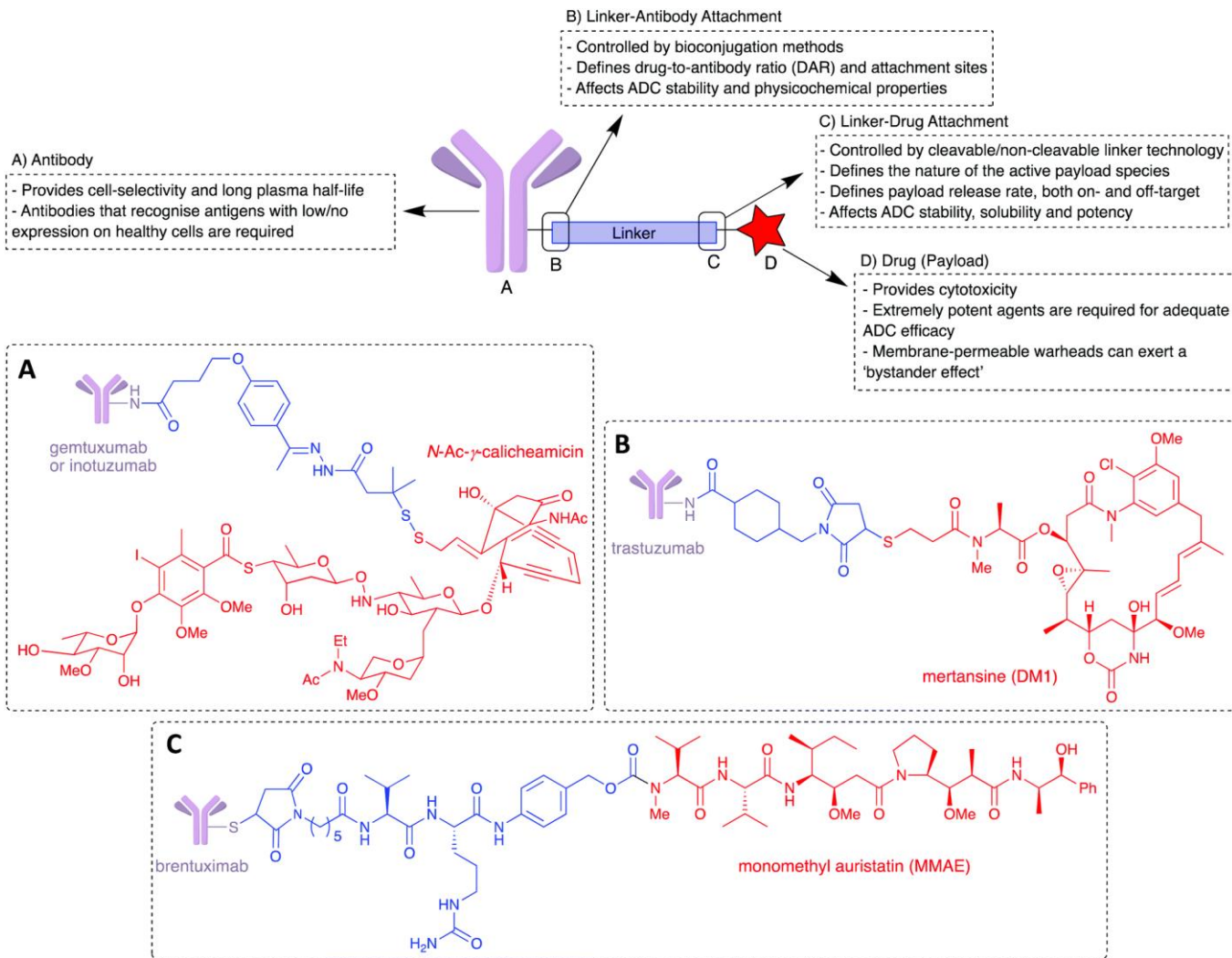


Fig. 1 (top) The general structure of an ADC and the role of each component. (bottom) The chemical structures of the four currently FDA-approved ADCs with the linkers in blue and the payloads in red.

(A) gemtuxumab ozogamicin (Mylotarg®) and inotuzumab ozogamicin (Besponsa®) (B) trastuzumab emtansine (Kadcyla®) (C) brentuximab vedotin (Adcetris®).

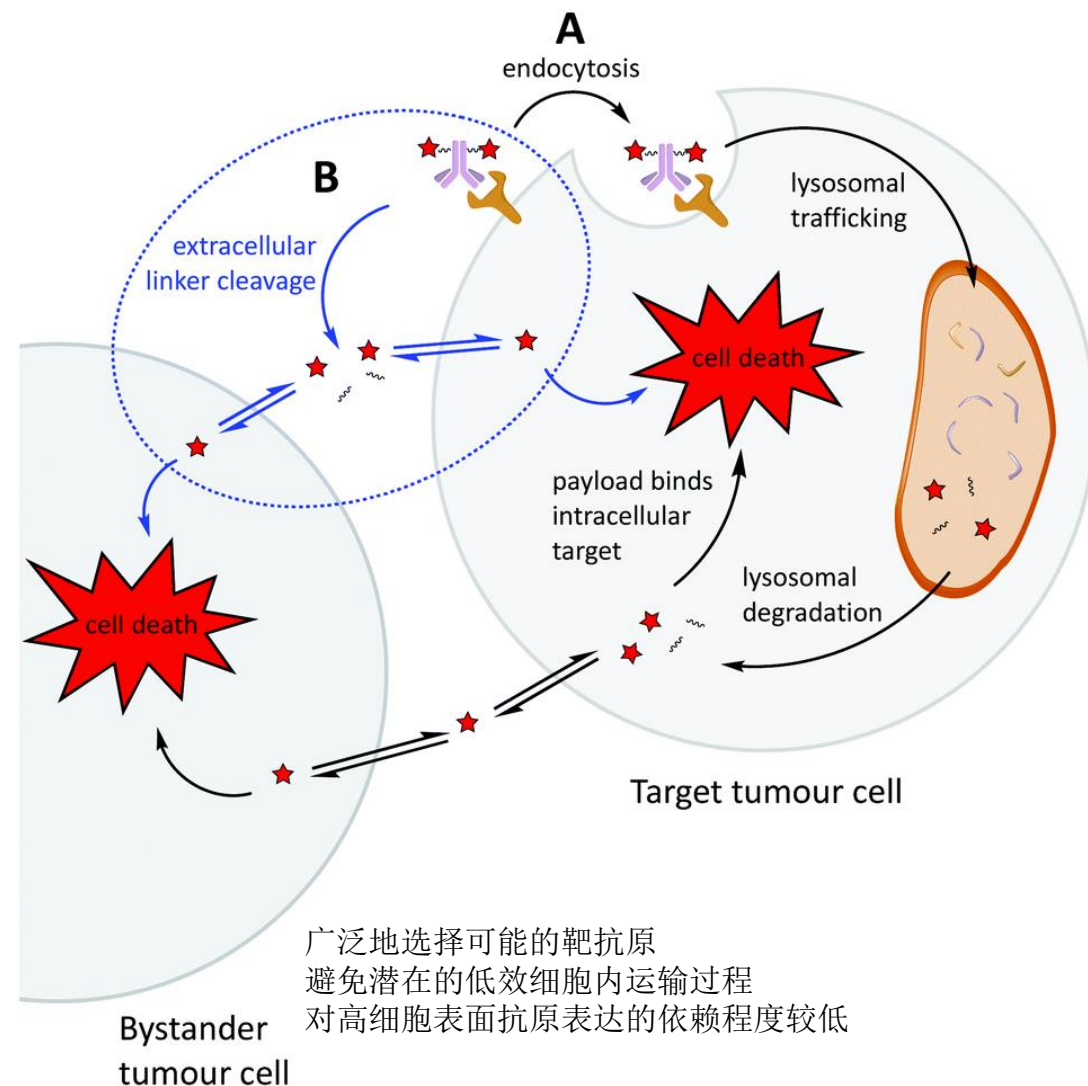
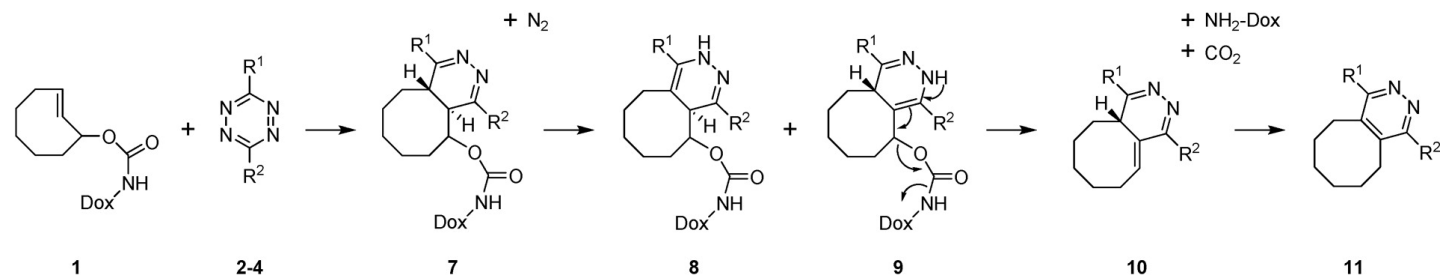
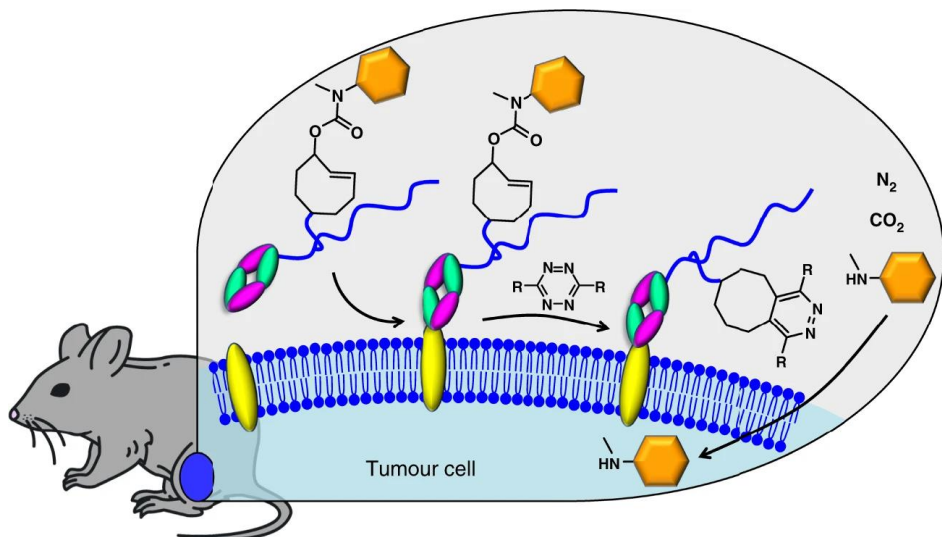


Fig. 2 (A) The traditional mechanism of action, involving endocytosis and intracellular payload release. (B) The non-internalising, extracellular mechanism of action.

Chemical- or light-mediated decaging of prodrugs

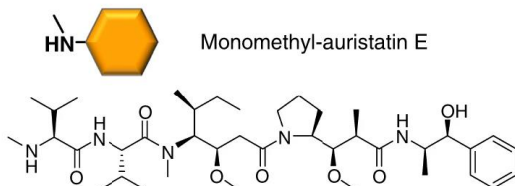


Bioconjugate Chem. 2016, 1697–1706.



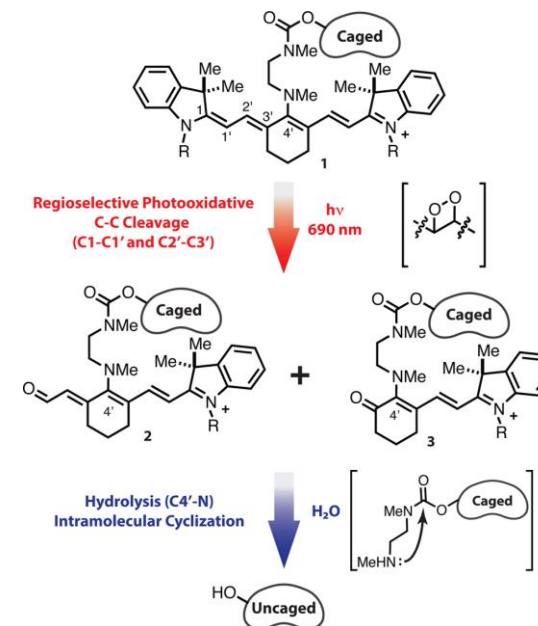
Anti-TAG72
diabody

Polyethylene-
glycol



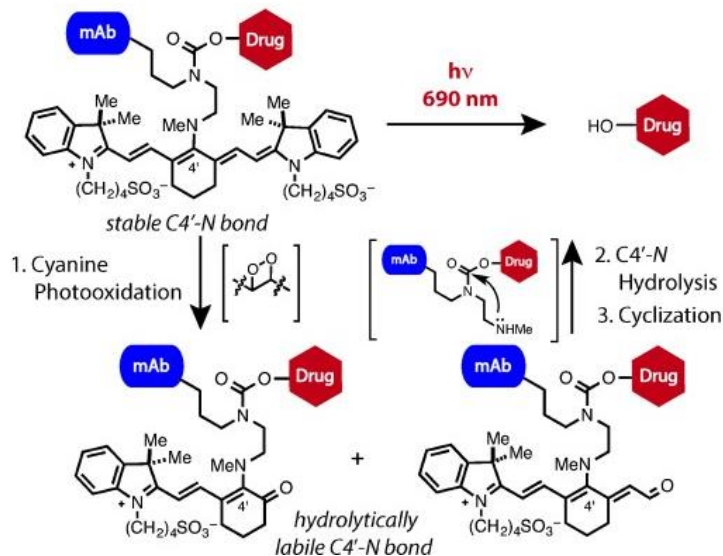
Triggered drug release using “click-to-release” chemistry in vivo: on-tumour liberation of a cell permeable drug (monomethyl auristatin E, MMAE) from a trans-cyclooctene-linked ADC following systemic administration of a tetrazine activator

Nat. Commun. 2018, 9, 1484.



J. Am. Chem. Soc. 2014, 136, 14153–14159.

B. Cyanine-Based Near-IR Cleavable Linker - Design and Mechanism



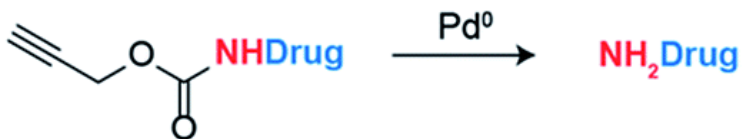
Design and mechanism of a cyanine-based near-IR light cleavable ADC.

Angew. Chem., Int. Ed. 2015, 54, 13635–13638.

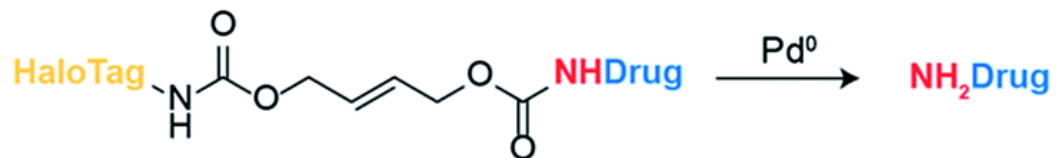
Metal-mediated decaging of prodrugs

Previous work

a Decaging of terminal propargyl carbamates (cells and mice)

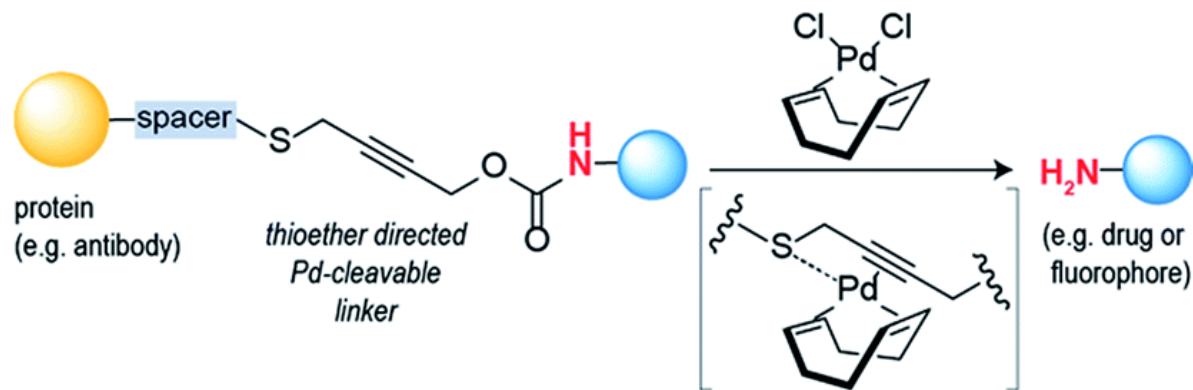


b Decaging of bifunctional allyl carbamates (cell lysates)



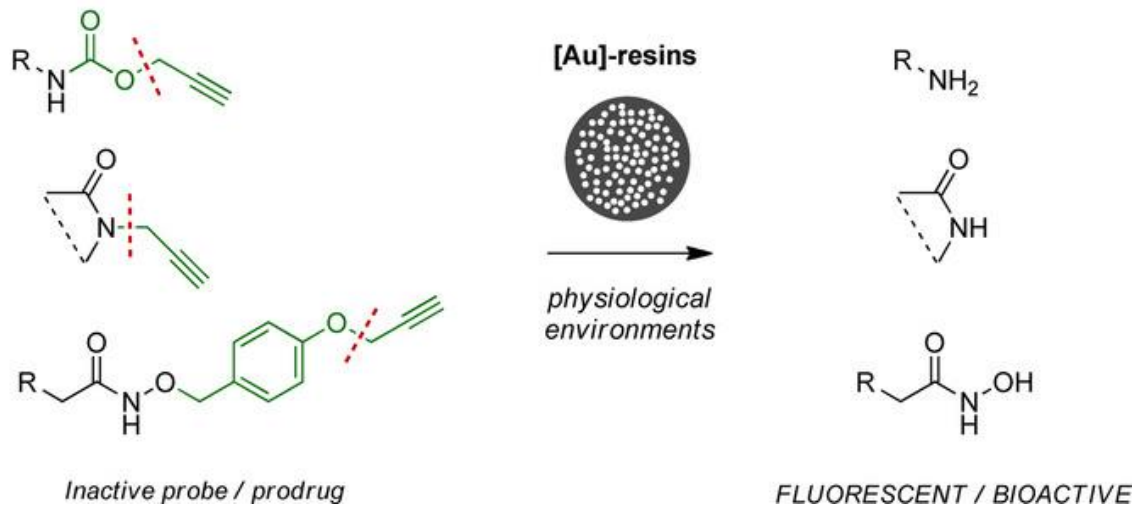
This work

c Decaging of bifunctional propargyl carbamates (cancer cells)

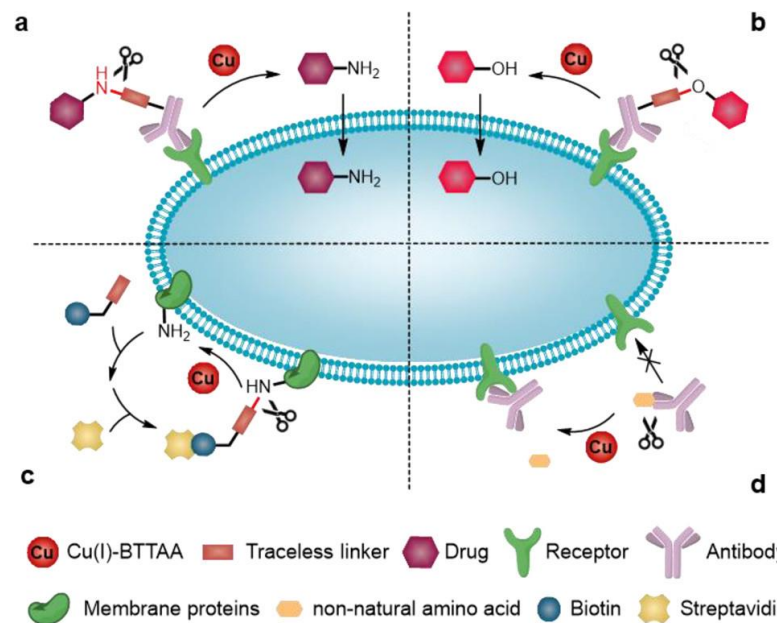


Chem. Sci. 2018, 9, 4185–4189.

b) This work - gold-triggered uncaging chemistry

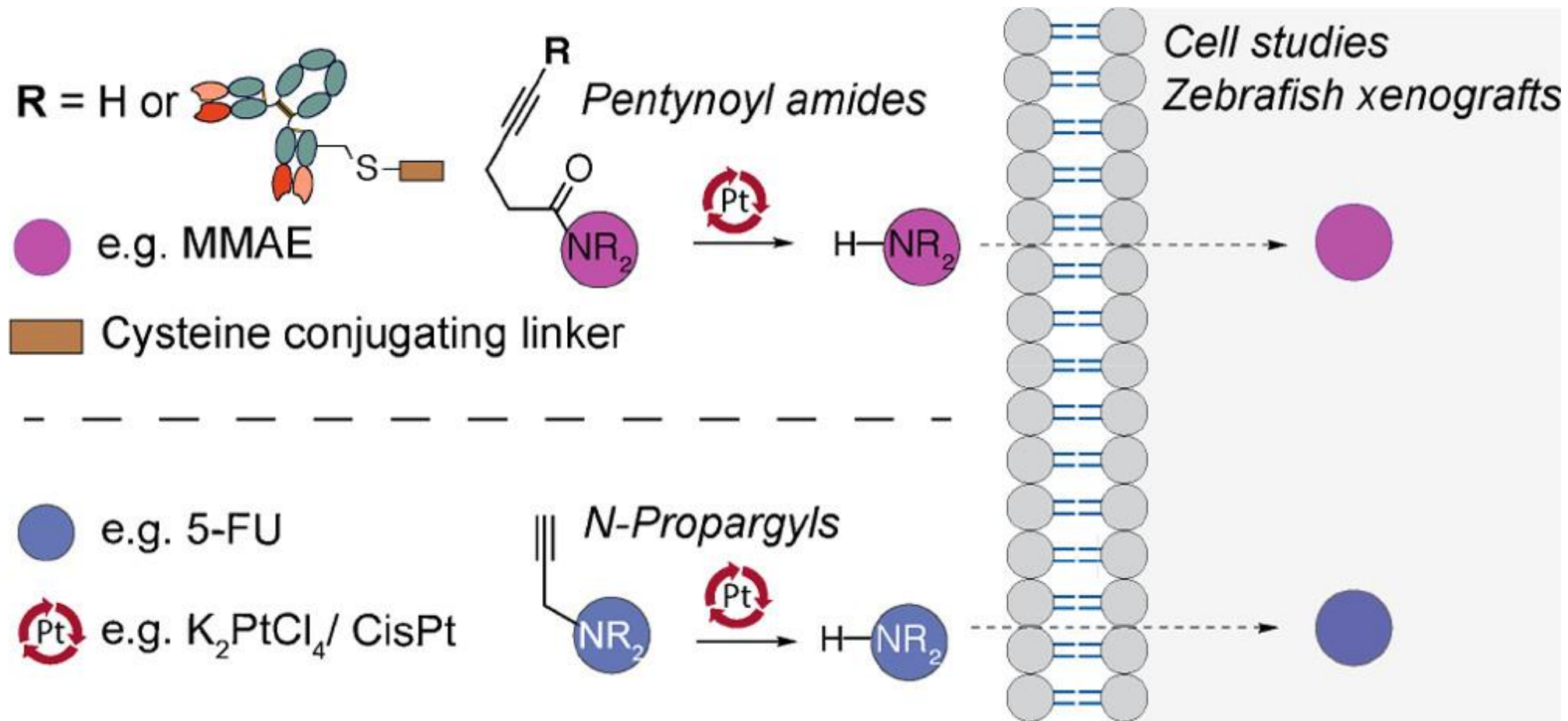


Angew. Chem., Int. Ed. 2017, 56, 12548–12552.



J. Am. Chem. Soc. 2019, 141, 17133–17141.

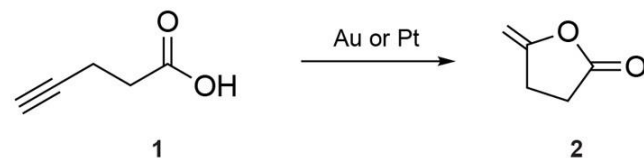
Platinum-Mediated Bioorthogonal Bond Cleavage



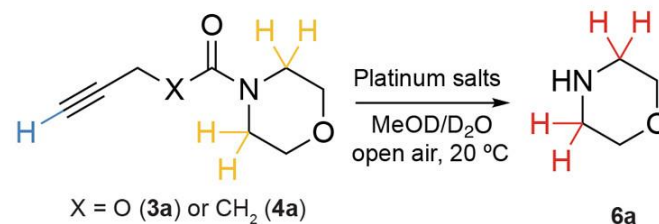
Secondary amines protected in the form of a tertiary pentynoyl amide (top) or N-propargyl (bottom) can be selectively deprotected by platinum reagents like the chemotherapeutic drug CisPt. This strategy was explored for drug activation of the protected MMAE and 5-FU drugs and extended for drug release from an ADC in cancer cells. Ultimately, CisPt-mediated activation of a “5-FU-propargyl prodrug” was evaluated in a zebrafish xenograft model for treatment of colorectal cancer.

Engineering of a Platinum-Mediated Decaging Reaction

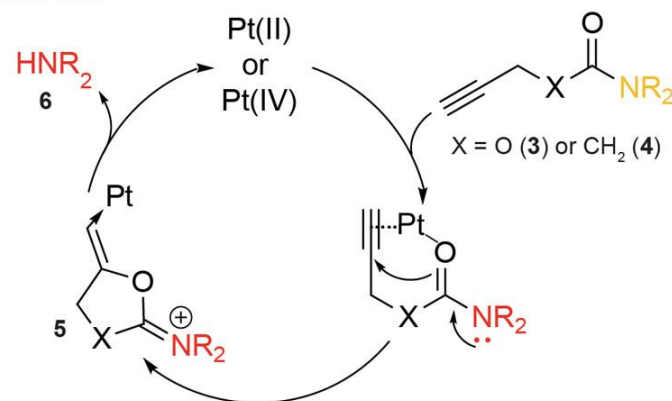
a Previous work



c Catalytic decaging of tertiary amides



b This work



d Conversions

Entry	Metal	Equiv.	Compound	Conversion % ^a
1	K ₂ PtCl ₄	0.1	3a	20 ± 6
2	K ₂ PtCl ₄	2.0	3a	61 ± 1
3	K ₂ PtCl ₄	0.1	4a	37 ± 1
4	K ₂ PtCl ₄	2.0	4a	50 ± 1
5	K ₂ PtCl ₆	0.1	4a	43 ± 3
6	K ₂ PtCl ₆	2.0	4a	81 ± 7

^a monitored by NMR

e Conversion rates over time for tertiary amide 4a in the presence K₂PtCl₄ (2 eq.)

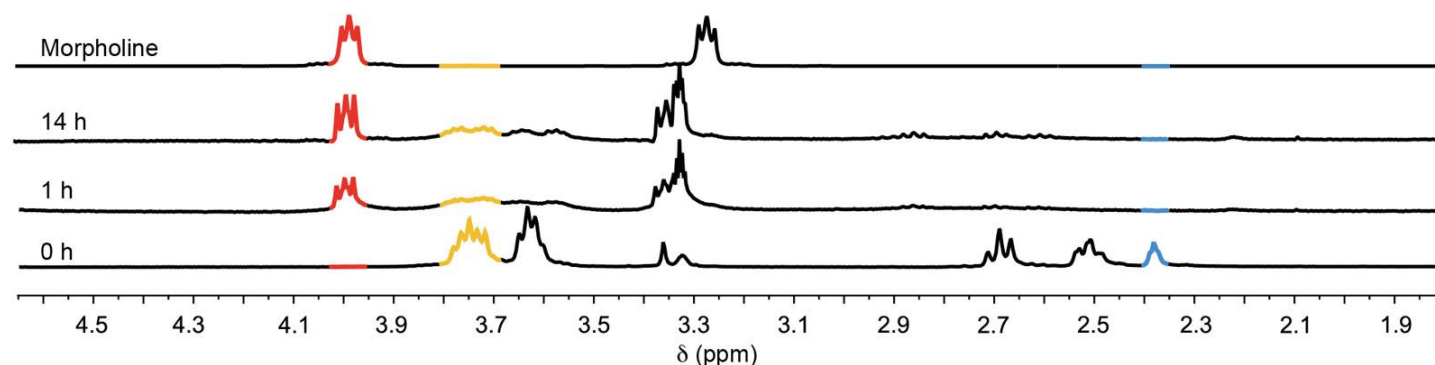


Figure 1. Platinum-mediated decaging reaction engineering. a. The cyclization of 4-pentynoic acid is known to proceed rapidly in aqueous media with gold and platinum complexes. b. The proposed reaction uses a carboxamide as an internal nucleophile that cyclizes and displaces the secondary amine leaving group, which could be a drug or a fluorophore. c. Model compounds with alkyne amide or carbamate were used to survey the decaging reaction. d. Efficiency of the cleavage reaction under different conditions was assessed by ¹H NMR spectroscopy. e. ¹H NMR spectroscopy of the decaging of the tertiary amide 4a in the presence of a catalytic amount of K₂PtCl₄. The reaction generates a cyclized intermediate that undergoes hydrolysis to release morpholine 6a. General procedure for determining decaging conversion by ¹H NMR spectroscopy: carbamate and amide compounds (10 mgs) were dissolved in MeOD (0.2 mL) and metal complexes (0.1 or 2 equiv) were added in D₂O (0.6 mL) at room temperature in an open vessel for 14 h. The reactions were transferred to an NMR spectroscopic tube and sealed. Conversion was calculated based on the relative ratios of methylene peaks resulting from the starting material and the released amine product. Numerical data are the mean of 2 or 3 replicates.

Mechanistic and Kinetic Studies of the Platinum-Mediated Decaging Reaction

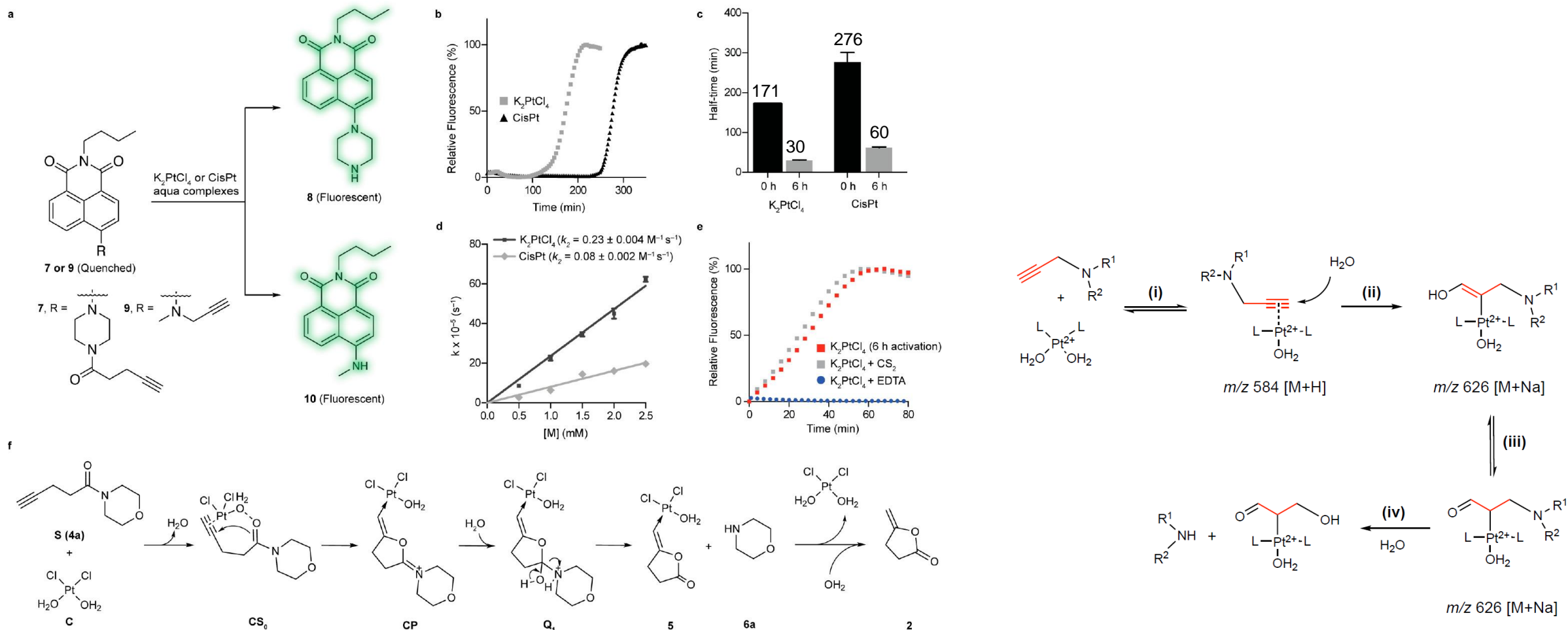


Figure 2. Examination of the platinum-catalyzed bioorthogonal cleavage reaction. **a**. Naphthalimide-based fluorogenic probes were used to study the cleavage efficiency of the platinum reaction for decaging alkyne-containing molecules. The caged naphthalimide derivatives exhibited high stability in solution and cell media and their quenched fluorescence could be reactivated upon removal of the caging group ($\lambda_{ex} = 445 \text{ nm}$, $\lambda_{em} = 545 \text{ nm}$). **b**. Changes in fluorescence intensity during the time course of the decaging reaction between fluorogenic probe 7 and platinum salts (K_2PtCl_4 /CisPt). **c**. Determined half-time for the reaction of 7 with activated and nonactivated platinum salts. **d**. Decaging kinetics for the pentynoyl amide fluorophore. Rate constants were determined under pseudo first order conditions with a $50 \mu\text{M}$ final concentration of probe 7 and 10–50 equiv of aqua platinum metals. **e**. Kinetics profiles of the decaging reaction in the presence of the metal poisons CS_2 and EDTA. Error bars represent \pm s.d. ($n = 3$). All experiments were repeated 3 independent times. **f**. Calculated mechanism for the depropargylation reaction catalyzed by Pt with model substrate 4a. Calculations were performed with an implicit solvent model for water. Geometries and frequencies were calculated with the functional revPBE and, to obtain very accurate energetics, single point energy calculations with DLPNO-CCSD(T) and counterpoise corrections were employed to suppress basis set superposition errors.

Platinum-Mediated Decaging in Living Cells

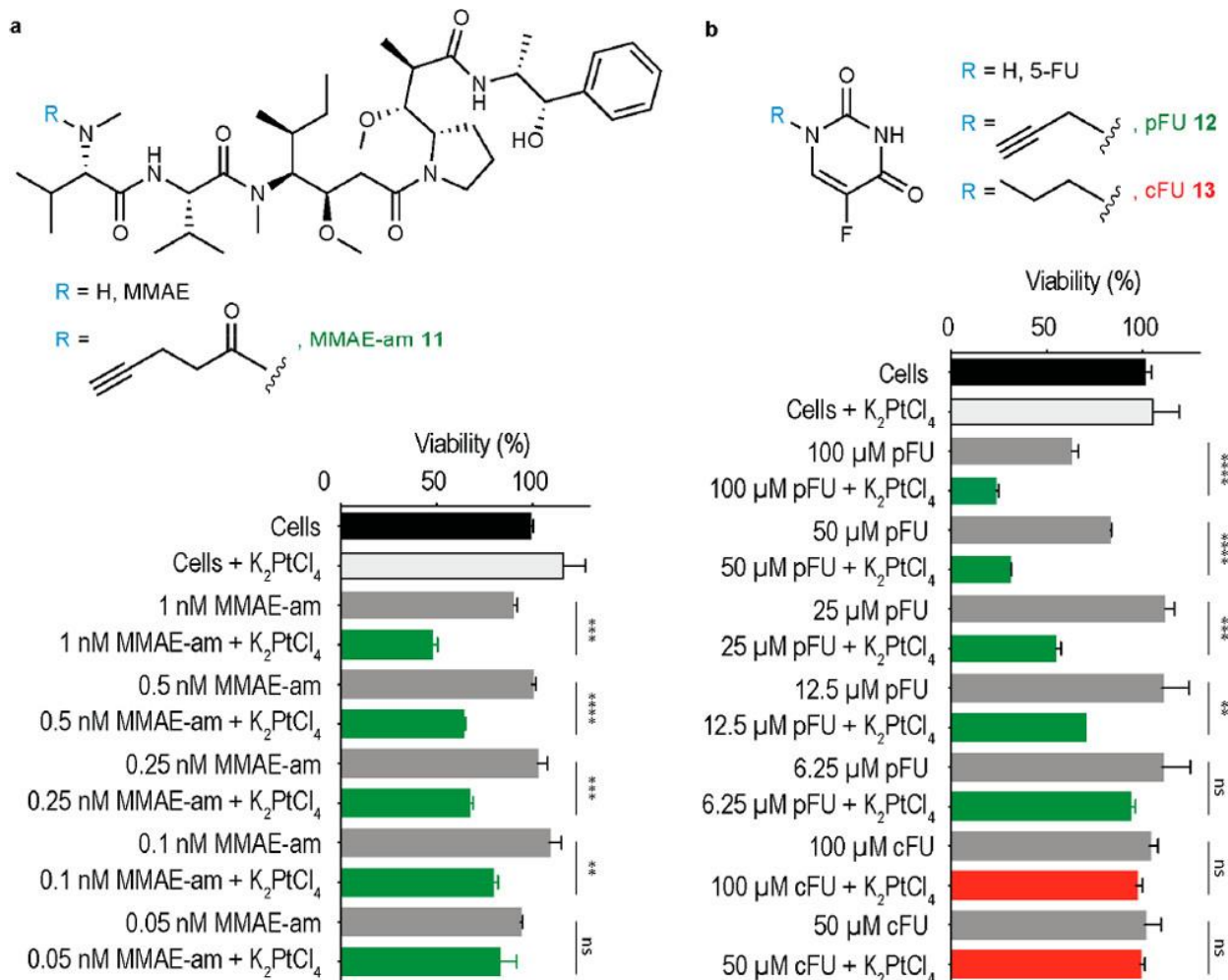


Figure 3. Platinum-mediated decaging in cells. HeLa cells were incubated with different concentrations of MMAE-am 11a or pFU 12b for 3 days with or without K₂PtCl₄ (20 μM, twice a day). Compound 13, a nondecaging alkyl-FU derivative, was used as a negative control. Toxicity was determined by AlamarBlue assay. Error bars represent \pm s.d. (n = 3). Each experiment was repeated three times. The statistical significance of the differences between groups was evaluated with the unpaired t test. Statistical results: ns > 0.05, **P ≤ 0.01, ***P ≤ 0.001 and ****P ≤ 0.0001.

Platinum Decaging of ADC

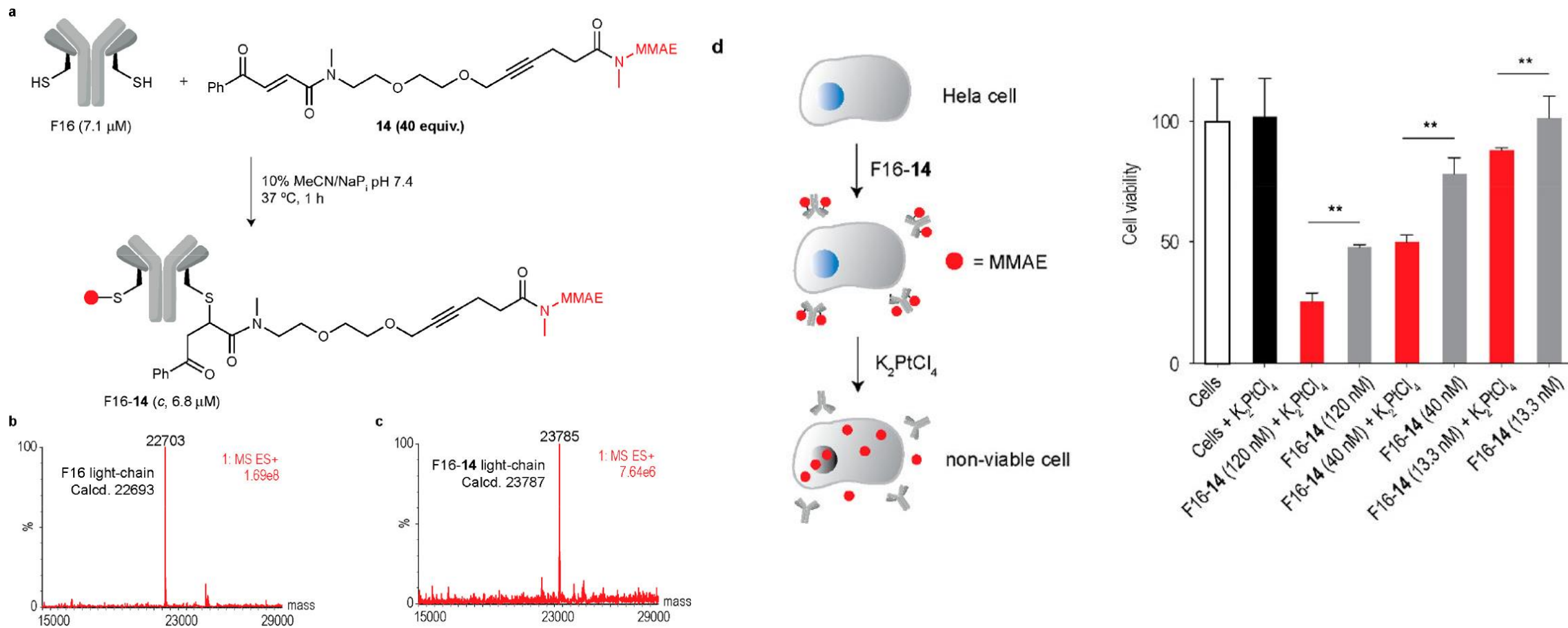


Figure 4. Platinum-mediated drug decaging from a noninternalizing ADC. a. Cysteine-selective and irreversible modification of the noninternalizing antibody F16 (anti tenascin-C) in IgG format with MMAE conjugating linker 14. IgG(F16) contains a single reactive cysteine at the C-terminal extremity of the light chain ideal for cysteine-specific modification. Briefly, a solution of F16 (7.1 μ M) in sodium phosphate buffer (NaPi) pH 7.4 was treated with 14 (40 equiv) in MeCN to a final concentration of 10% v/v. The reaction was heated to 37 $^{\circ}$ C for 1 h, and reaction progress was monitored by LC-MS. The ADC was purified by dialysis into fresh NaPi buffer pH 7.4 with a 10 kDa MWCO overnight. b. Deconvoluted ESI-MS mass spectrum of the light-chain of F16. c. Deconvoluted ESI-MS mass spectrum of the light-chain of F16-14 that shows an exact drug-to-light-chain ratio of 1. d. Schematic of the platinum-mediated decaging of MMAE from a noninternalizing ADC. e. Cell viability of HeLa cells after treatment with F16-14 and subsequent decaging efficiency upon treatment with 20 μ M K_2PtCl_4 , twice daily. Cell viability was measured at day 3 by using AlamarBlue reagent. The statistical significance of the differences between groups was evaluated by using the unpaired t test. A p value <0.05 (***) was considered statistically significant. Error bars represent \pm s.d. (n = 3). Experiments were performed three times.

Cisplatin-Mediated Prodrug Decaging in Vivo

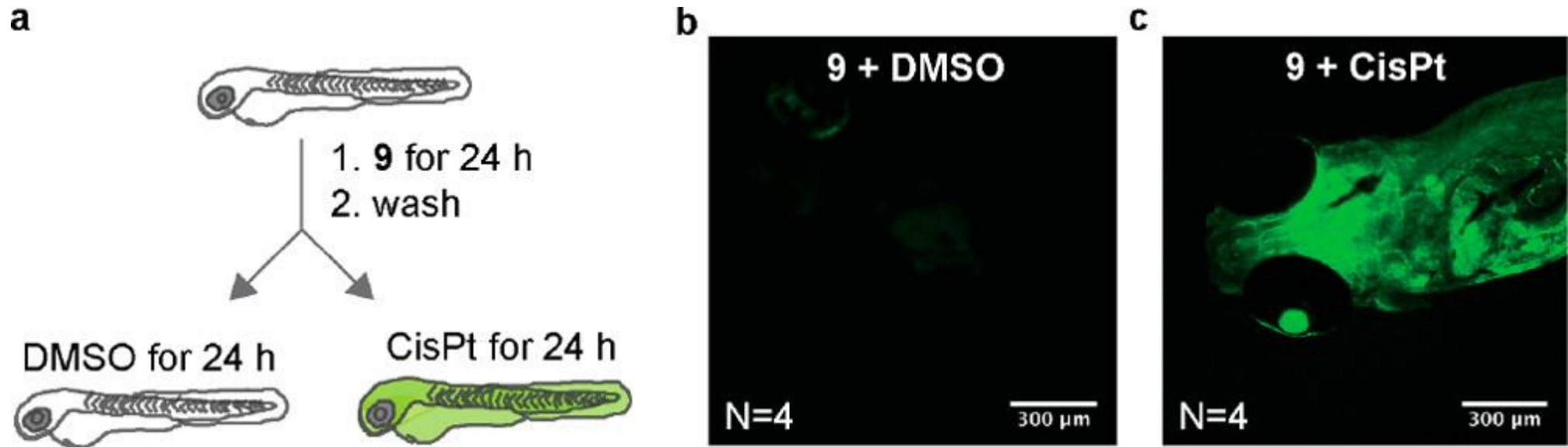


Figure 5. CisPt Decages the Fluorogenic Probe 9 in vivo. Zebrafish larvae were exposed to 9 diluted in embryonic medium for 24 h, followed by a 1 h wash in embryonic medium. Larvae were randomly distributed into two conditions: DMSO or CisPt for 24 h (a). Confocal image of zebrafish larvae exposed to 9 + DMSO (b) and 9 + CisPt (c).

Cisplatin-Mediated Prodrug Decaging in Vivo

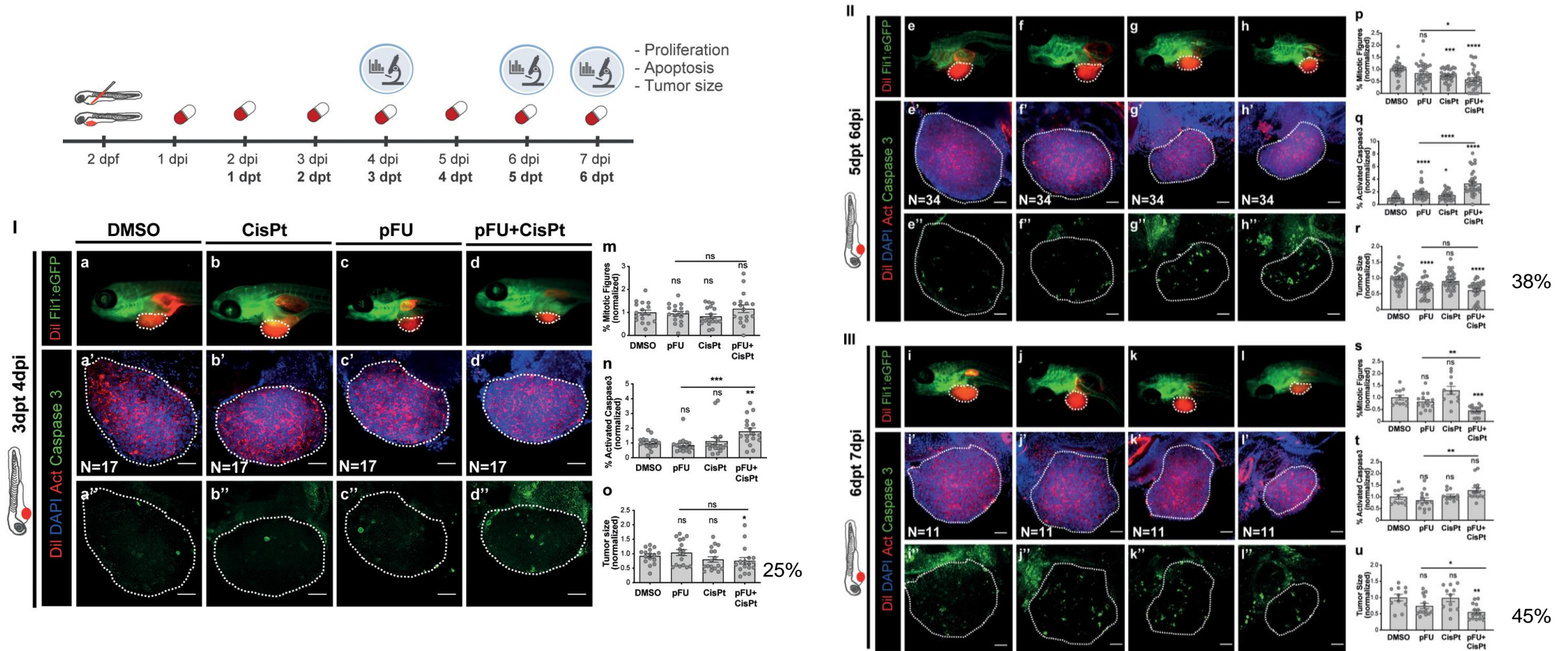


Figure 6. CisPt-mediated prodrug decaging in zebrafish xenografts. HCT116 human CRC cells were fluorescently labeled with lipophilic CM-DiI (shown in red) and injected into the perivitelline space (PVS) 2 days post fertilization (dpf) Tg(Fli1:eGFP) zebrafish larvae. Zebrafish xenografts were randomly distributed into treatment groups, daily treated with DMSO, CisPt, pFU, and pFU+CisPt and analyzed at 4, 6, or 7dpi for proliferation, apoptosis and tumor size. At 4 dpi, 6 dpi, and 7dpi, zebrafish xenografts were imaged by stereoscope (a–l) and by confocal microscopy (a'–l' DAPI plus DiI, a''–l'' maximum projection of activated caspase 3). Proliferation (mitotic figures: m; p, *P = 0.0104, ***P = 0.0004, ****P < 0.0001; s, **P = 0.0023, *** P = 0.0002), apoptosis (activated caspase 3: n, **P = 0.0033, ***P = 0.0006; q, *P = 0.0126, ****P < 0.0001; t, **P = 0.0068) and tumor size (n° of tumor cells: o, *P = 0.0279; r, ****P < 0.0001; u, *P = 0.0411, **P = 0.0010) were analyzed and quantified. Graphs represent fold induction (normalized values to controls) of Avg ± SEM. The number of xenografts analyzed is indicated in the representative images and each dot represents one zebrafish xenograft. Statistical analysis was performed using an unpaired test. Statistical results: ns > 0.05, *P ≤ 0.05, **P ≤ 0.01, ***P ≤ 0.001, and ****P ≤ 0.0001. All images are anterior to the left, posterior to right, dorsal up, and ventral down. Scale bar 50 μm.